# Einstein Beams: Optical Beams Following Gravitationally Lensed Trajectories

Enrique J. Galvez and Jake M. Freedman

Department of Physics and Astronomy, Colgate University, Hamilton, New York 13346, U.S.A.

#### ABSTRACT

We use a spatial light modulator (SLM) to mimic the effect of gravity and steer the light from a laser to observe Einstein rings with a laboratory camera. The derived programming of the phase of the SLM follows a logarithmic dependence with impact parameter. As expected, we also observe arcs when the source and lensing object are not in line with the observer. Measurements for distinct parameters are consistent with the expectations. The coherent optical beams that are programmed to follow gravitational lensing trajectories have a transverse mode consistent with Bessel functions, yet they do not exhibit the non-diffracting properties of Bessel beams: they expand linearly with the propagation distance. The addition of a vortex phase also produces patterns that coincide with Bessel modes of order given by the topological charge of the vortex.

# 1. INTRODUCTION

The defiction of light due to a gravitating body was first considered by Johann Soldner in 1801. He predicted that a light ray passing near the Sun should be deflected by an angle of 0:85 arcsec. More than a hundred years later Albert Einstein made a similar prediction based on Newtonian mechanics, which he updated later to 1:74 arcsec using his theory of general relativity. Eddington verified Einstein prediction in a famous solar eclipse in 1919, which led to wide recognition of Einstein's theory. In 1924 Chwolson first pointed out that if there was perfect alignment between a background star and light-deflecting foreground star, it would produce a ring-like image around the foreground star. This was possibly the birth of the concept of gravitational lensing, but after Einstein made a comment on those rings in a paper in 1936, they became called, perhaps unfairly, "Einstein rings." Observational verifications of gravitational lensing started in the radio<sup>2</sup> and continue to this day with stunning optical observations by the Hubble Space Telescope and other modern instruments. A The initial research also expanded to the inhomogeneous lensing due to galaxies and clusters, as first suggested by Zwicky, and more recently, in the search for dark matter. The inhomogeneities of galaxies and dark matter lead to the appearance of caustics and multiple images. It is also important to note that microlensing, though not involving imaging, plays an important role in the study of exoplanets.

Simulation of gravitational lensing has been of much interest for pedagogical purposes, 9-11 but also in research simulations of the phenomenon, involving platforms such as optical fibers, 13 metamaterials, 14, 15 and transformational optics. 16 There is much interest in simulating lensing and other effects caused by a black hole. 16-18 In this article we use a spatial light modulator (SLM) to mimic the most simple cases of strong lensing with symmetric lensing objects: rings and arcs. One part of the article describes this simulation of rings and arcs. However, in doing this work we stumbled on an interesting situation, which was afforded by the flexibility of the SLM in conjunction with coherent light beams. It led us to finding a new type of optical beams. We call these "Einstein" beams because they are created by the light rays following the gravitationally lensed trajectories. Thus in the second part of the article we make an analysis of the beams, and the effects of adding orbital angular momentum to them.

Further author information: E.J.G.: E-mail: egalvez@colgate.edu (Send correspondence to E.J.G.)

E.J.G.: E-mail: egalvez@colgate.edu, Telephone: 1 315 228-7205

To appear in Proceedings of SPIE 11701 (2021).

# 2. SIMULATING EINSTEIN RINGS

## 2.1 Strong Lensing Using a Simulated Schwarzschild Lens

We consider the setup shown in the Fig. 1, a point source on the axis of the object-lens-observer, following previous analyses.<sup>1,19</sup> The angles are very small in reality. For example, gravitational lensing objects subtend angles of 30 arcsec or less.<sup>1</sup> These angles are likely to be small in the lab as well. Using the small angle approximation, for  $\alpha \ll 1$ , we get from Fig. 1:

$$D_{\rm SI}\theta = D_{\rm SL}\alpha,\tag{1}$$

where  $D_{\rm SI}$  and  $D_{\rm SL}$  are the distances from the source to image and source to lens, respectively.

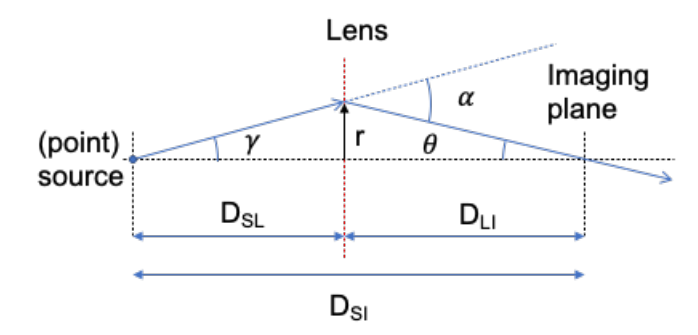


Figure 1. Geometry of the problem and the relevant parameters for simulating the gravitational lens by a point mass.

The angle  $\alpha$  is known from general relativity:

$$\alpha = \frac{2r_S}{r},\tag{2}$$

where r is the impact parameter, and  $r_S$  the Schwarzschild radius of the point mass M, given by

$$r_S = \frac{2GM}{c^2},\tag{3}$$

with G being the gravitational constant, M is the mass of the lensing object, and c is the speed of light. The previous approximation is equivalent to  $r \gg r_S$ .

If we eliminate r from Eqs. 1 and 2 and solve for  $\theta$ , we get the expression for the Einstein ring.

$$\theta_E = \sqrt{\frac{2D_{\rm SL}r_S}{(D_{\rm SL} + D_{\rm LI})D_{\rm LI}}}.$$
(4)

We note a few particular cases:

1. When  $D_{\rm SL} \gg D_{\rm LI}$ 

$$\theta_E = \sqrt{\frac{2r_S}{D_{\rm LI}}}. (5)$$

This is the most likely case in cosmological observations of strong lensing.

2. When  $D_{\rm SL} \sim D_{\rm LI}$ 

$$\theta_E = \sqrt{\frac{2r_S}{2D_{\rm LI}}}. (6)$$

This is a case that we can easily set up in the optical laboratory, and which may correspond to some cases of microlensing.

In both cases the Einstein radius has a simple dependence with  $D_{\rm LI}$ , and hence, location of the observer.

# 2.2 SLM programming

We present the rationale for programming the SLM by first considering the case of a simple lens, followed by the gravitational problem.

#### 2.2.1 Lens Focusing

A lens that focuses an expanding beam follows the picture seen in Fig. 2. The phase differential of the incoming paraxial light wave at a point a distance r from the axis of the lens is

$$d\phi_1 = k\gamma dr \tag{7}$$

and similarly for the outgoing beam

$$d\phi_2 = -k\theta dr \tag{8}$$

where k is the wavenumber.

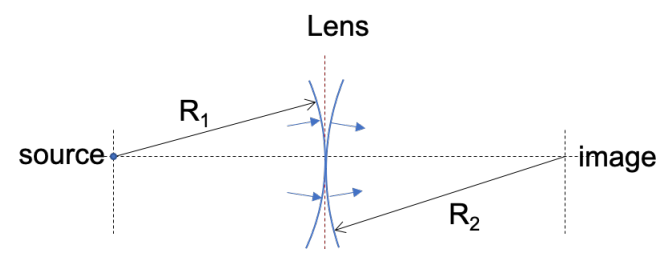


Figure 2. Imaging by a regular lens.

Thus, the lens (SLM) adds a phase

$$d\phi_{\text{SLM}} = d\phi_2 - d\phi_1 \tag{9}$$

$$d\phi_{\text{SLM}} = d\phi_2 - d\phi_1$$

$$= -k \frac{r}{D_{\text{SL}}} dr - k \frac{r}{D_{\text{SL}}} dr$$

$$(9)$$

and where we used

$$\gamma \simeq \frac{r}{D_{\rm SL}} \tag{11}$$

and

$$\theta \simeq \frac{r}{D_{\rm LI}},$$
 (12)

as seen in Fig. 1. Integrating Eq. 10 with  $\phi_{\text{SLM}_{-}0} = 0$  for r = 0 we get

$$\phi_{\rm SLM} = -\frac{kr^2}{2D_{\rm LI}} - \frac{kr^2}{2D_{\rm SL}}.$$
 (13)

Imaging by a lens follows the well-known relation:

$$\frac{1}{R_2} = \frac{1}{R_1} - \frac{1}{f},\tag{14}$$

where  $R_1$  and  $R_2$  are the radii of curvature of the wavefront, with the convention that the value of the radius is R > 0 when the center of curvature is to the left of the wavefront, and conversely R < 0 when it is on the right, as shown in Fig. 2. Therefore, we can apply Eq. 14 by using  $R_1 = D_{\rm SL}$  and  $R_2 = -D_{\rm LI}$ , and get

$$\phi_{\text{SLM}} = \frac{kr^2}{2} \left( \frac{1}{R_2} - \frac{1}{R_1} \right)$$

$$= -\frac{kr^2}{2f}.$$
(15)

$$= -\frac{kr^2}{2f}. (16)$$

Note that the final phase is independent of the input and output radii of curvature, and depends only on the focal length of the lens, showing that the programmed SLM replaces a real lens for any imaging situation.

#### 2.2.2 Gravitational Lensing

In the case of a gravitational lens the rays are not all refocused to a single point as they would with an ordinary lens. It is more like Fig. 3(a). Thus,  $d\phi_2$  in Eq. 8 should use:

$$\theta = \alpha - \gamma \tag{17}$$

yielding

$$d\phi_2 = -kdr\alpha + kdr\gamma \tag{18}$$

Note that when replacing into Eq. 10 there is a fortuitous cancellation, leading to

$$\phi_{\text{SLM}} = -\int_{r_0}^r \frac{2kr_S}{r} dr = -2kr_S \ln\left(\frac{r}{r_0}\right),\tag{19}$$

where we have used  $\phi_{\text{SLM}=0} = 0$  for  $r = r_0$ . The phase produces a beam of rays that focus at shallower angles as the impact parameter r increases, as shown in Fig. 3. Note then that due to the cancellation, the programming of the SLM does not depend on the angle of the input ray.

#### Source Far Away

Let us consider first the case when  $D_{SL} \to \infty$ , and assume that at  $r_E$  we get the deflection that causes the Einstein ring. The values of expected experimental parameters are as follows.

- The wavenumber is:  $k \sim 10^7 \text{ m}^{-1}$
- For a phase change on the SLM that is not higher than the resolution, we pick  $2kr_S = 125$ .
- This results in  $r_S = 6.25 \ 10^{-6} \ \mathrm{m}$
- We also pick an observation point D=2 m.
- Because

$$\alpha_E = \frac{2r_S}{r_E} = \frac{r_E}{D} \tag{20}$$

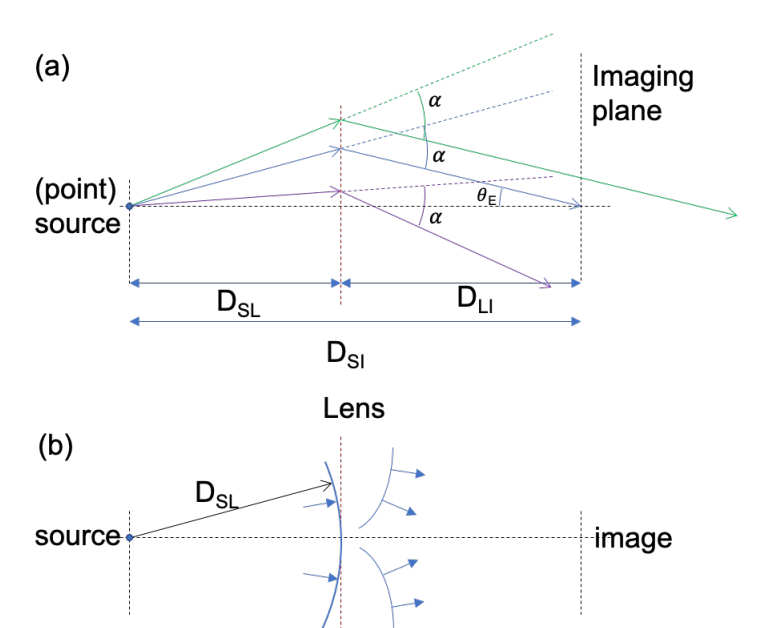


Figure 3. (a) Gravitational lensing for rays with different impact parameters; (b) Wavefronts reaching and leaving the gravitational lens.

we calculate

$$r_E = \sqrt{2r_S D} = 5 \ 10^{-3} \ \text{m} \tag{21}$$

and so  $\alpha_E = 2.5 \ 10^{-3} \ \mathrm{rad}$ .

- In imaging the Einstein ring, as shown in Fig. 4, we have the following parameters:
  - If f = 0.1 m, the Einstein radius seen with the camera is  $r_C = f\alpha_E = 2.5 \ 10^{-4}$  m
  - The pixel conversion for our camera is c = 1280/0.0066 pix/m, so  $r_C = 48.5$  pix
  - If we decide for a different observation point  $D_M=1.5$  m, the impact parameter for the observed Einstein ring is  $r_M=\sqrt{2r_SD_M}=0.00433$  m
  - The Einstein angle for this measurement is  $\alpha_M = 2r_S/r_M = 0.00289$
  - The radius in the camera is  $r_C = f\alpha_M = 0.000289 \text{ m} = 56 \text{ pix}$

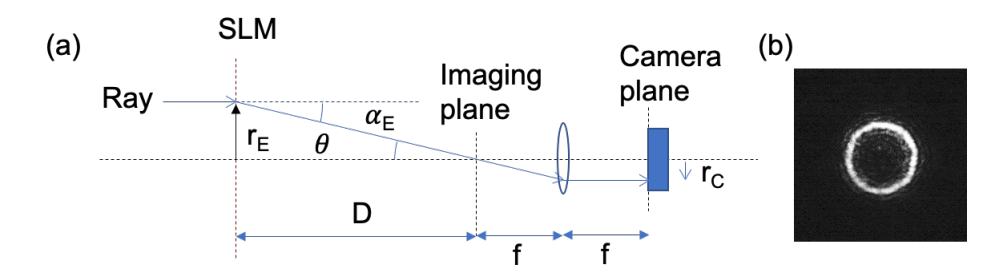


Figure 4. (a) Schematic of the imaging of the Einstein ring, consisting of an aperture, a lens and a camera. (b) Actual image taken with the camera.

# 2.3 Apparatus

The apparatus used to take the data is shown in Fig. 5. A Pair of lenses spatially filtered the light from a Helium Neon laser to produce either a parallel beam or to focus it before the SLM to mimic a "near" source object. The SLM was programmed as explained above, with a logarithmic radial phase. A 4-f system was used to re-image the SLM at a convenient location. Einstein rings were measured with an imaging unit consisting of a small aperture followed y a lens and camera, each separated a focal length away. The whole beam was imaged by a second camera.

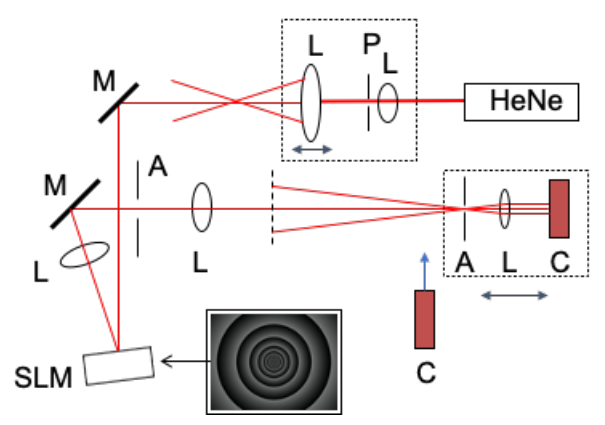


Figure 5. Apparatus to create Einstein beams. Optical components include lenses (L) pinhole (P) apertures (A), mirrors (M), camera (C) and spatial light modulator (SLM). Insert shows an example of the phase programming of the SLM.

#### 2.4 Measurement Results

Figure 6 shows a linearized graph of measurements relating the square of the diameter of the rings as a function of two lensing parameters: central mass and observation distance. The agreement between the measurements and the expectations is excellent.

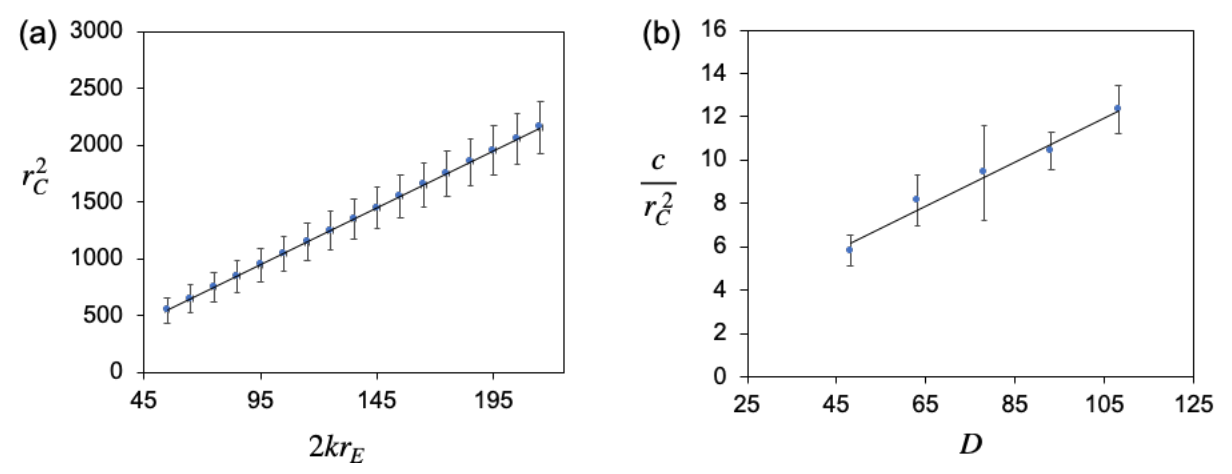


Figure 6. The camera measured an Einstein radius  $r_C$ : (a) Graph of measurements as a function of the lensing mass, proportional to  $2kr_E$ ; (b) Graph of the measurements as a function of the propagation distance (in m), where  $c = 15^5$  is a scaling constant.

#### 3. OFF-AXIS LENSING

## 3.1 Ray Tracing

Now we consider the situation where the source, lensing mass and observer are not along the same line, as shown in Fig. 7(a). We will use a geometrical construction that is different than used previously,  $^{1,19}$  to best suit the laboratory geometry that uses the SLM, where the beam remains fixed and the lens' center is displaced. In the most simple form, this situation is analyzed from the plane of symmetry that contains the 3 main points of the problem. It gives rise to two images of the source, appearing at angles  $\theta_1$  and  $\theta_2$  from the direction of the lensing mass. From the observer'e point of view, the lensing (point) mass M forms an angle  $\beta$  with the direction of the source. Here we find the angles of the two images.

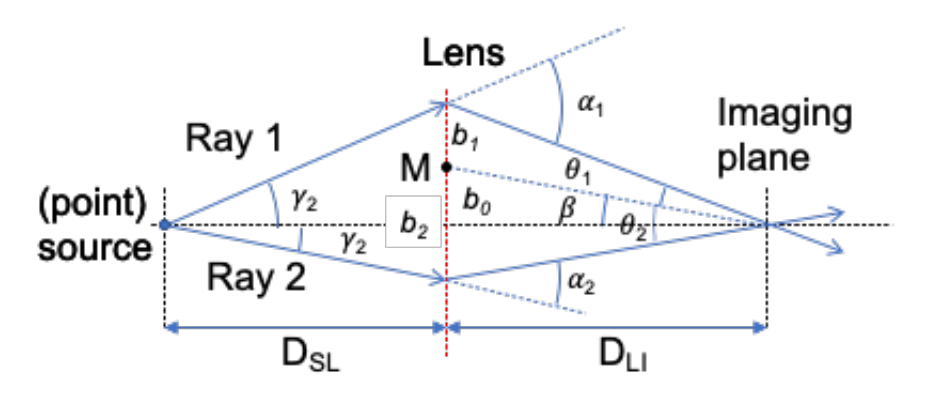


Figure 7. (a) Off-axis ray-tracing geometry. (b) Image taken with the setup described by shifting the lensing mass.

#### 3.1.1 Ray 1

Applying the small angle approximation for ray 1 we have the following relation:

$$\theta_1 + \beta = \frac{\gamma_1 D_{\rm SL}}{D_{\rm LI}},\tag{22}$$

where

$$\gamma_1 = \alpha_1 - (\theta_1 + \beta),\tag{23}$$

with

$$\alpha_1 = \frac{2r_S}{\theta_1 D_{\text{LI}}}. (24)$$

This leads to

$$(\theta_1 + \beta) \left( 1 + \frac{D_{\rm SL}}{D_{\rm LI}} \right) = \frac{2D_{\rm SL} r_S}{\theta_1 D_{\rm LI}^2} \tag{25}$$

or

$$\theta_1 + \beta = \frac{2D_{\rm SL}r_S}{\theta_1 D_{\rm LI}(D_{\rm LI} + D_{\rm SL})}.$$
 (26)

When  $\beta = 0$  this reduces to  $\theta_1 = \theta_E$ , the Einstein radius of the aligned situation, given by Eq. 4. In the off-axis situation Eq. 26 reduces to a quadratic equation

$$\theta_1^2 + \beta \theta_1 - \theta_E^2 = 0. (27)$$

The solution with a positive angle is

$$\theta_1 = \frac{\sqrt{\beta^2 + 4\theta_E^2} - \beta}{2}.\tag{28}$$

#### 3.1.2 Ray 2

A similar analysis for ray 2 gives

$$\theta_2 - \beta = \frac{\gamma_2 D_{\rm SL}}{D_{\rm LI}},\tag{29}$$

where

$$\gamma_2 = \alpha_2 - (\theta_2 - \beta),\tag{30}$$

with

$$\alpha_1 = \frac{2r_S}{\theta_2 D_{11}},\tag{31}$$

leading similar algebraic manipulations to reach

$$\theta_2 - \beta = \frac{2D_{\rm SL}r_S}{\theta_2 D_{\rm LI}(D_{\rm LI} + D_{\rm SL})}.$$
(32)

This gives rise to another quadratic equation, now for  $\theta_2$ :

$$\theta_2^2 - \beta \theta_1 - \theta_E^2 = 0, (33)$$

with positive solution given by

$$\theta_2 = \frac{\sqrt{\beta^2 + 4\theta_E^2} + \beta}{2}.\tag{34}$$

There is a nice symmetry to Eqs. 28 and 34, with  $\theta_2 > \theta_1$ . That is, the source produces two images that are at the two sides of the central mass at unequal angles. If additionally we make  $\beta << \theta_E$ , then

$$\theta_1 \simeq \theta_E - \frac{\beta}{2} \tag{35}$$

$$\theta_2 \simeq \theta_E + \frac{\beta}{2}.$$
 (36)

Both images are formed approximately symmetrically about the Einstein angle. This can be seen in the image taken in the laboratory, shown in Fig. 8(b). The dashed line shows the location of the Einstein ring. A fit of a circle that passes through the two arcs yields a displaced center. Since the arcs are displaced by  $\beta/2$ , the fitted center of the circle passing through the arcs should vary linearly with the displacement of the location of the lensing mass. This is exactly what is seen in the laboratory, as shown in Fig. 8(b)

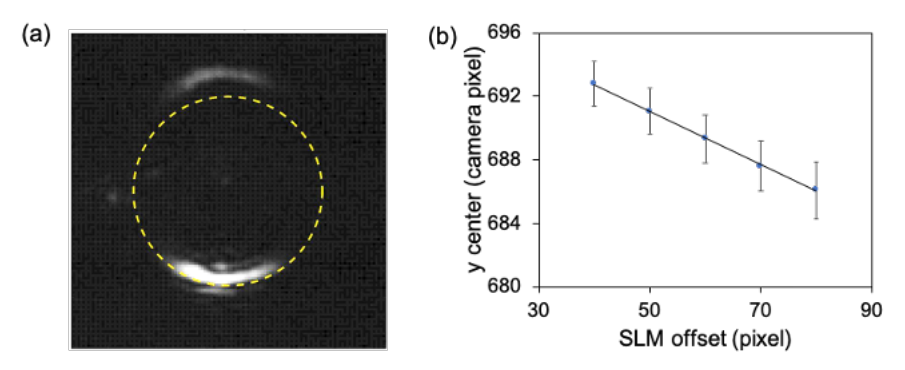


Figure 8. (a) Einstein arcs produced by displacing the location of the lensing mass vertically. Dashed line is the location of the ring with no displacement, Data and fit of the center of the two arcs as a function of the position of the location of the lensing object in the SLM.

#### 4. EINSTEIN BEAMS

## 4.1 Measurements

In gravitational lensing with cosmic sources we only see the light reaching Earth, but in our case we are recreating it with a coherent source that we can manipulate and image in a plane of observation. Thus it begs the question what beam pattern do we get? The beam that is observed is shown in Fig. 9. The profiles look conspicuously similar to Bessel beams, although they are not formed the same way, so we call them Einstein beams. The SLM can impart a phase vortex onto the beam. The images in (a) and (b) of Fig. 9 correspond to no azimuthal phase, and an azimuthal phase with topological charge  $\ell = 3$ , respectively.

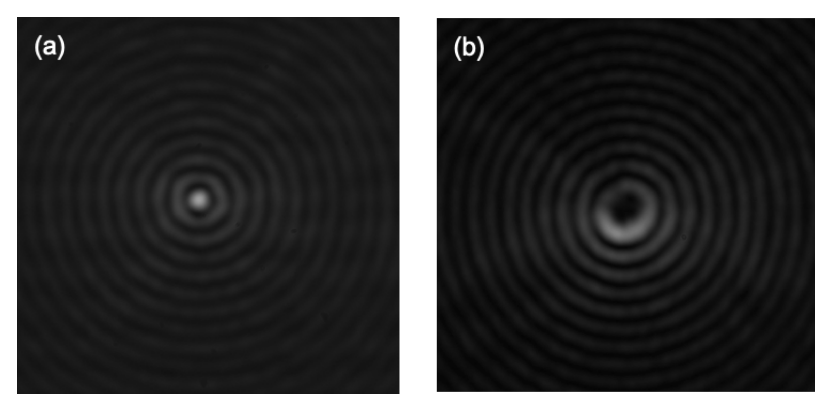


Figure 9. Images of Einstein beams with topological charges  $\ell = 0$  (left) and  $\ell = 3$  (right).

Figure 10 shows several analyses we made of Einstein beams. In Fig. 10(a) we show a 2-dimensional fit of the intensity with a 2-dimensional Bessel beam. This is representative of many others that we did. It shows that the minima coincide with the minima of Bessel beams. The intensity pattern matches that of the a Bessel function squared, in all parts except on the center, where the data is always lower than the predicted value. Measurements for different points along the propagation direction show that the beam expands linearly. This is shown in Fig. 10(b) via a fit of the first minima of the patterns as a function of the propagation distance.

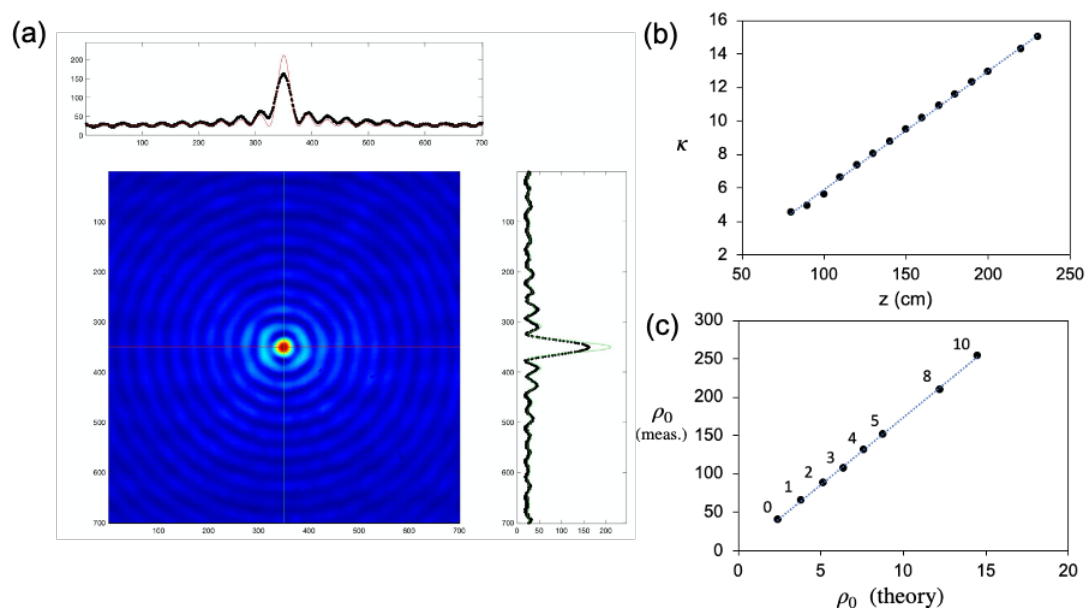


Figure 10. Analysis of Einstein beams: (a) Fit of a 2-dimensional Bessel function fit to the data for  $\ell = 0$ ; (b) Graph of the Bessel parameter  $\kappa$  (Eq. 38) as a function of the propagation distance; (c) Graph of the measured first zero of the Bessel beam  $\rho_0$  of different topological charge graphed against the theoretical value.

A linear curve fits very well to the data. We investigated further the dependence with topological charge. We found that the first minima coincide with the first zero of the Bessel function of the same order as the topological charge, as shown in Fig. 10(c).

#### 4.2 Heuristic Theory

A rigorous approach to analyze Einstein beams is the angular decomposition.<sup>21</sup> However, a simple argument can be made where the variation of the angular inclination of the rays producing a given image is nearly constant and given by  $\theta = r_E/D_{\rm LI}$ , but considering  $r_E$  to constant just for the sake of getting an approximate result. If the topological charge is  $\ell$ , this leads to the standard expression for a Bessel beam

$$U \propto e^{i(kz+\ell\phi)} J_{\ell}(\kappa\rho) \tag{37}$$

with  $(\rho, \phi)$  being the polar coordinates in the transverse plane and

$$\kappa = \frac{kr_E}{D_{\rm LI}}.\tag{38}$$

Thus the previous equation gives a Bessel profile that expands with  $D_{\rm LI}$ .

#### 5. DISCUSSION

We presented a method to simulate gravitational lensing using an SLM. We have initially concentrated on point lensing objects, resulting in observed Einstein rings and arcs that are consistent with the expectations. The results open a path for simulating lensing from more complex objects featuring asymmetries, as is the case of lensing from galaxies, clusters and dark matter. It can also allow for more detailed studies of the corresponding caustics.<sup>2</sup> Although microlensing does not involve imaging, we can use the SLM to make similar types of simulations for the detection of exoplanets. These investigations can also focus on lensing by black holes.

A somewhat unexpected outcome of the work was the coherent beams that are generated by the gravitationally lensed trajectories of rays in coherent beams. The versatility of the SLM allows the easy insertion of an azimuthal phase (i.e., an optical vortex). Our observation of beams with Bessel profiles is not surprising in retrospect, as

rays producing a given image are nearly parallel, with inclination that decreases with the propagation distance, leading to an expanding Bessel profile of order equal to the topological charge imparted by the SLM. This provides another setting for investigations of gravitational lensing by rotating Kerr black holes, which contain non-zero orbital angular momentum.<sup>22,23</sup>

#### ACKNOWLEDGMENTS

This work was funded by NSF grant PHY2011937. We thank Warner Miller for motivating discussions.

#### REFERENCES

- [1] Schneider, P., Ehlers J. and Falco, E.E. Gravitational Lenses (Springer-Verlag, Berlin, 1992).
- [2] Blandford, R.D., and Narayan, R. "Cosmological applications of gravitational lensing," *Annu. Rev. Astron. Astrophys.* **30**, 311-358 (1992).
- [3] Treu, T., "Strong lensing by galaxies," Annu. Rev. Astron. Astrophys. 48, 87–125 (2010).
- [4] Treu, T., Marshall, P.J., and Clowe, D. 11Resource letter GL-1: gravitational lensing," Am. J. Phys. 80, 753–763 (2012).
- [5] Zwicky, F. "Nebulae as gravitational lenses," Phys. Rev. 51, 290 (1937).
- [6] Ellis, R.S., "Gravitational lensing: a unique probe of dark matter and dark energy," *Phil. Trans. R. Soc. A* **368** 967-987 (2010).
- [7] Gaudi, B.S., "Microlensing surveys for exoplanets," Annu. Rev. Astron. Astrophys., 50, 411–453 (2012).
- [8] Tsapras, Y. "Microlensing searches for exoplanets," em Geosciences 8, 365 (2018)
- [9] Liebes, S. "Gravitational lens simulator," Am. J. Phys. 37, 103–104 (1969).
- [10] V. Icke, "Construction of a gravitational lens," Am. J. Phys. 48, 883-886 (1980).
- [11] J. Higbie, "Gravitational lens," Am. J. Phys. 49, 652-655 (1981).
- [12] M. Falbo-Kenkel and J. Lohre, "Simple gravitational lens demonstrations," Phys. Teacher 34, 555-557 (1996).
- [13] Philbin, T.G., Kuklewicz, C., Robertson, S., Hill, S., König, F., and Leonardt, U., "A fiber-optical analog of the event horizon," *Science* **319**, 1367–1370 (2008).
- [14] Genov, D.A., Zhang, and S., Zhang, X., "Mimicking celestial mechanics in metamaterials," Nat. Phys. 5, 687-692 (2009).
- [15] Sheng, C., Liu, H., Wang, Y., Zhu, S.N., and Genov, D.A. "Trapping light by mimicking gravitational lensing," *Nat. Photon.* 7, 902–906 (2013).
- [16] Chen, H., Miao, R.-X., and Li, M., "Transformation optics that mimics the system outside a Schwarzchild black hole," *Opt. Express* **18**, 15183–15188 (2010).
- [17] Barceló, C. "Analogue black-hole horizons," Nat. Phys. 15, 210–213 (2019).
- [18] Belgiorno, F., Cacciatori, S.L., Clerici, M., Gorini, V., Ortenzi, G., Rizzi, L., Rubino, E., Sala., V.G., and Faccio, D. "Harking radiation from ultrashort laser pulse filaments," *Phys. Rev. Lett.* **105**, 203901 (2010).
- [19] K. Kuijken "The Basics of Lensing," APS Conference Series, 2003.
- [20] Nandor M.J., and Helliwell, T.M. "Fermat's principle and multiple imaging by gravitational lenses," Am. J. Phys. 64, 45-49 (1996).
- [21] Gbur, G.J. Singular Optics (Taylor & Francis, 2017).
- [22] Tamburini, F., Thidé, B., Molina-Terriza, G., and Anzolin, G. "Twisting of light around rotating black holes," Nat. Phys. 7, 195-197 (2011).
- [23] Tamburini, F., Thidé, B., and Della Valle, M. "Measurement of the spin of the M87 black hole from its observed twisted light," MNRAS 492, L22-L27 (2020).